This article has been accepted for publication in IEEE Transactions on Magnetics. This is the author's version which has not been fully edited and content may change prior to final publication. Citation information: DOI 10.1109/TMAG.2025.3536185

# Evaluation of the feasibility of TMR sensor array vertical packing for enhanced detectivity

Filipe Favita*, Pedro D. R. Araujo*†, Francisco Matos*†, Susana Cardoso*†, Paulo P. Freitas*†,
* INESC Microssistemas e Nanotecnologias, INESC-MN, Lisbon, Portugal
† Instituto Superior Técnico, Universidade de Lisboa, Portugal

***Abstract*—Increasing the number of vertically packed magnetic sensors in parallel has been proposed to improve field detectivity. However, the practical implementation of these ultra-compact architectures suffers from the increased surface roughness and magnetic coupling between the TMR levels, which can negatively impact the sensor's performance. To mitigate these effects, several strategies are evaluated in this work: aligned, shifted, and alternating integration of the TMR arrays. Moreover, different free layer sensitivities are explored, using NiFe and CoFeBSi free layers. Among these, the optimized geometry is shown to be two-level TMR sensors distributed in an alternating geometry that demonstrated superior performance to single level TMR arrays, achieving a detectivity of 3.9 nT·Hz$^{-1/2}$ with a NiFe free layer and 8.3 nT·Hz$^{-1/2}$ at 10 Hz with a CoFeBSi-based free layer.**

## I. Introduction

Development of devices with high signal-to-noise ratio, low power consumption, and a small footprint is indispensable for measuring magnetic fields created in biological systems, which are in the pT and fT range with frequencies around 10 mHz to 1 kHz [1], [2]. Although various devices can be developed based on different sensing principles, magnetoresistive sensors present a competitive compromise between device footprint and detectivity [3]—the ability to measure the smallest magnetic fields at specific frequencies. Among these, TMR sensors are particularly advantageous due to their higher sensitivity compared to Anisotropic Magnetoresistance AMR [4] and GMR sensors. Previous work show successful integration of GMR sensors in a compact architecture, using vertical packing [5]. In this work, we focus on vertically integrating TMR sensors in parallel to achieve lower detectivity. Diverging from conventional sensor design strategies that rely on creating 2D arrays [6], this approach preserves a compact footprint, crucial for high spatial resolution where xMR technologies excel [7].

Sensors vertically integrated in parallel can theoretically detect smaller magnetic fields due to a decrease in detectivity. If one considers a sensor array of $n_Y$ branches in parallel with $n_X$ MTJs in series, stacked vertically a $n_Z$ number of times, there will be a scaling in sensitivity with $n_X$, whilst noise voltage spectral density will have a dependency with $\sqrt{n_X/n_Y n_Z}$ within the thermal voltage regimen. Therefore, when comparing equivalent $n_X$, $n_Y$ arrays with a number $n_Z$ of vertically stacked sensors in parallel, a decrease in detectivity with $n_Z^{-1/2}$ is expected.

Vertical packing is an interesting approach to achieve lower detectivity because it minimizes the device's footprint by moving to the Z axis in the fabrication process, iterating it an $n_Z$ number of times. Due to this vertical repetition, an increase in topography occurs as documented by [8]. To try to minimize this effect, vertical integration strategies were also implemented aiming to minimize the overlap of the sensing regions: shifted and alternating strategy, whereas the aligned strategy serves as the control.

Each vertical integration (represented in Fig.1) consists in:

- Vertical alignment between MTJs and bottom electrodes of even and odd levels - Alternating Strategy Fig.1.[1]
- Shifted Pillar structure with aligned bottom electrodes - Shifted Strategy Fig.1.[2]
- Vertical alignment between MTJs of different levels - Aligned Strategy Fig.1.[3].

Two of these strategies aim to minimize roughness in the new levels packed vertically since the TMR stack is deposited on top of the previous level. Going from the aligned to shifted and then alternating strategy, there is an increasing distance between the newly defined pillar regions and the pillar region of the previous TMR layer. For instance, we move from a perfect alignment in design in the aligned strategy (Fig.1.[3.A]), to a decreasing overlap in the pillar structures between even and odd levels of the shifted strategy (Fig.1.[2.A]), and minimum overlap for the alternating strategy (Fig.1.[1.A]).

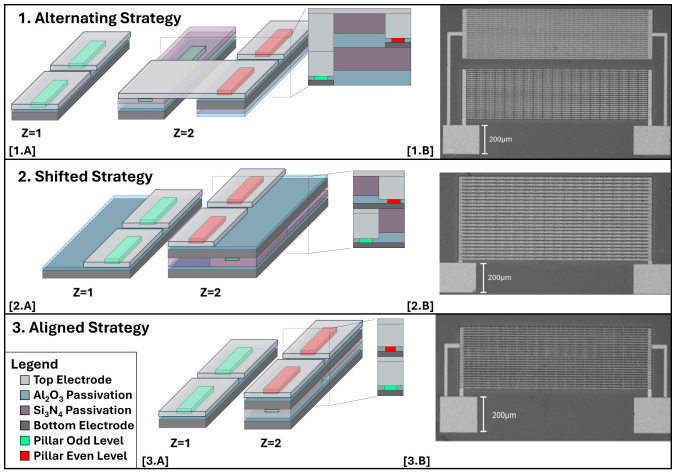


Fig. 1: Schematic of the integration strategies and its cross-section: Aligned [1.A], Shifted [2.A] and Alternating [3.A]. In [1-3.B] the sensor's top view.

This article has been accepted for publication in IEEE Transactions on Magnetics. This is the author's version which has not been fully edited and content may change prior to final publication. Citation information: DOI 10.1109/TMAG.2025.3536185

## II. Experimental Method

To develop and vertically integrate TMR sensors, several microfabrication steps were repeated along the Z-axis, including defining the bottom electrode, pillar, and top electrode of the sensors, followed by $Si_3N_4$ interlayer passivation and via opening. The sensors were fabricated on a $Si/SiO_2$ substrate, with new parallel TMR levels vertically connected. Each TMR level contained sensors with single, arrays of 200 and 1000 MTJs using the specified packing strategies. Two different MgO-based TMR sensor multilayered stacks were deposited using Ion Beam Deposition (IBD) and magnetron sputtering in a Nordiko 3600/8800 tool: [Ru(10)/Ta(5)]x3/Ru(5)/Ta(5)/$Mn_{78}Ir_{22}$(8)/$Co_{70}Fe_{30}$(2.2)/Ru (0.65)/$Co_{40}Fe_{40}B_{20}$(2)/MgO(1.6)/FL/Ru(5)/Ta(5)/Ru(10) nm with FL for stack A $Co_{40}Fe_{40}B_{20}$(1.5)/Ru(0.2)/$Ni_{80}Fe_{20}$(4) nm and $Co_{40}Fe_{40}B_{20}$(2)/Ru(0.2)/$Co_{70.5}Fe_{4.5}B_{10}Si_{15}$(8) nm for stack B. After deposition, the bottom electrode and pillar structures were patterned by optical lithography and $Ar^+$ Ion Beam Milling (Nordiko 3600 tool), followed by 130 nm $Al_2O_3$ passivation (magnetron sputtering). The MTJ stack was patterned into 2x20 $\mu m^2$ rectangles to linearize the sensors through shape anisotropy [7]. Between TMR levels, 300 nm $Si_3N_4$ passivation was applied using Plasma-Enhanced Chemical Vapor Deposition in an Oxford tool, with vias opened through RIE (SPTS etcher) after DWL lithography. Each TMR layer was metalized with 130 nm $Al_{98.5}Si_{1.0}Cu_{0.5}$ and 15 nm $Ti_{12.5}W_{50}(N_{37.5})$ (magnetron sputtering, Nordiko7000 tool). To define the reference layer direction, each sample was vacuum-annealed at 330 °C for 2 hours under a 1T field.

The sensors were characterized magneto-electrically using a two-probe method (I = 10 $\mu A$). Measurements were made within an applied magnetic field range of [-20, 20] mT to determine the sensors' sensitivity. The noise spectra (10 Hz to 100 kHz) were acquired in a shielded environment using a spectrum analyzer and a low-noise amplifier [5], at the sensors' maximum sensitivity: H = 0 for sensors with stack B, with a linear range of [-8, 8] mT, and H = 1.5 mT using a permanent magnet for stack A, with a linear range around [-2, 4] mT.

## III. Experimental Results

A decrease in detectivity with the number of vertical levels can only be attained if both sensitivity and noise spectra scale accordingly to the dependencies refered. Focusing on the sensitivity evolution with vertically integrated TMR levels, Figs. 2.[A] and 2.[B] show an MR decrease from sensors with $n_Z$=1 to $n_Z$=2 in stack A and stack B, respectively, with a dependency on the integration strategy: an almost similar MR ratio between the alternating strategy and the sensor with $n_Z$=1, and the lowest MR for the aligned strategy where there is pillar and bottom electrodes alignment between TMR levels.

By performing a statistical dispersion of the extracted maximum sensitivity (i.e. slope) for each sensor, in Fig. 3 we observe a decrease in sensitivity both with the packing strategies level alignment, correlated with decreased MR, as well as with new vertically packed levels.

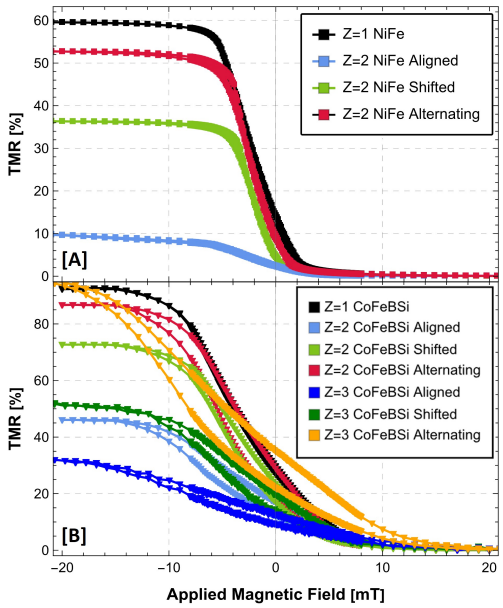


Fig. 2: Representative transfer curves of sensors and the respective strategies with arrays of 200 MTJs ($n_X = 20$ and $n_Y = 10$), for $n_Z = 1$, 2 stack A [A] and 3 for stack B [B]. In panel [A] sensors utilize stack A, while in [B] stack B.

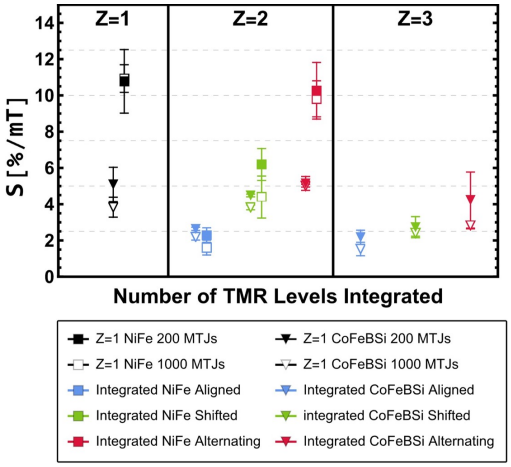


Fig. 3: Sensitivity distribution across sensors with different levels of TMR in parallel and integration strategies for both arrays of 200 MTJs ($n_X$=20, $n_Y$=10) and 1000 MTJs ($n_X$=25, $n_Y$=20) of the two different stacks. The error bar represents the standard deviation of the respective population.

The sensitivity decrease suggests that accumulation of roughness with each additional TMR level deteriorates sensor performance, this observation aligns with the integration strategies effectiveness [8]. Transitioning from aligned to shifted to alternating strategies results in decreasing overlap and misalignment between consecutive MTJs, consequently, MTJ stack deposition occurs on the least rough surface with the alternating strategy, the roughest surface with the aligned, and intermediate with the shifted approach, where between consecutive TMR levels the bottom electrodes are aligned but the pillars shifted. During TMR stack deposition, thin film

This article has been accepted for publication in IEEE Transactions on Magnetics. This is the author's version which has not been fully edited and content may change prior to final publication. Citation information: DOI 10.1109/TMAG.2025.3536185

growth and uniformity are affected accordingly, confirmed by comparing the integration strategies in Fig. 3, which shows the highest MR ratio for the alternating strategy, followed by shifted, and the lowest for the aligned strategy. Moreover, roughness may not be the only factor at play. The documented interlayer magnetic coupling in spin valves [5], also contributes to lower sensitivities in vertically integrated TMR sensors. The alternating strategy, with direct vertical alignment between odd and even levels, increases the vertical separation between TMR levels (from 300 nm to 860 nm), decreasing interlayer coupling, an advantage to other strategies.

Regarding the noise spectra, in Figs. 4.[A] and 4.[B] the spectra for 200 arrays of $n_Z$=1 and $n_Z$=2 of both stacks are displayed, as well as each sensor Thermal-Shot noise contribution which is overall in the same order of magnitude.

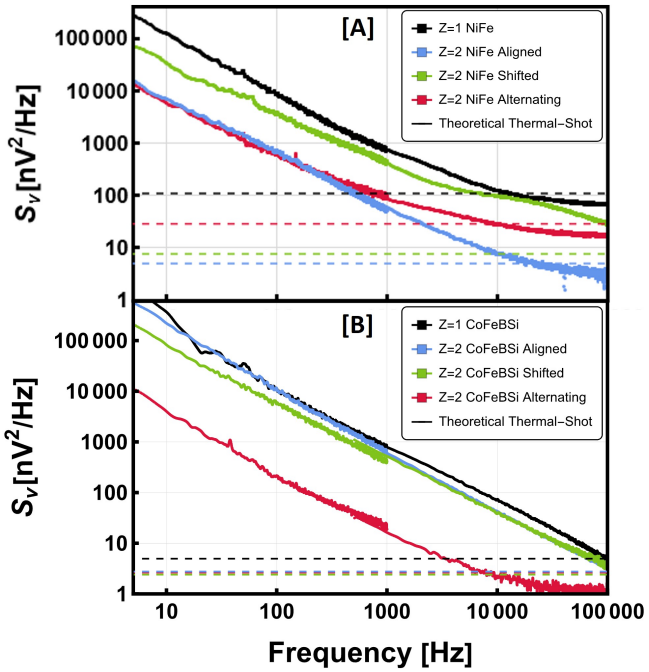


Fig. 4: Noise spectra of 200 MTJ arrays sensors (250 mV bias). [A] stack A measurements with 1.5 mT applied field. Minimum resistances: $n_Z$=1, $R_{min}$= 3.3 kΩ; $n_Z$=2, $R_{min}$= 150 Ω (aligned), 230 Ω (shifted), 862 Ω (alternating). [B] stack B measurements without an applied field. Minimum resistances: $n_Z$=1, $R_{min}$= 77 Ω; $n_Z$=2, $R_{min}$= 43 Ω (aligned), 37 Ω (shifted), 41 Ω (alternating).

Observing the noise spectra, there is a decrease in noise intensity in the packed systems across all the acquired frequency ranges. The shifted $n_Z$=2 sensor (stack A) still shows excessive noise intensity near 10 kHz due to a RTN contribution.

The detectivity spectra were obtained for the sensors of both stacks and are presented in Figs. 5.[A] and 5.[B] for, respectively, stack A and B. The noise and detectivity values would benefit from further analysis, including a correction factor obtained by electronic modeling as proposed in [9], enabling better comparison between our results and others in the literature.

Based on the figures, the alternating and shifted strategies

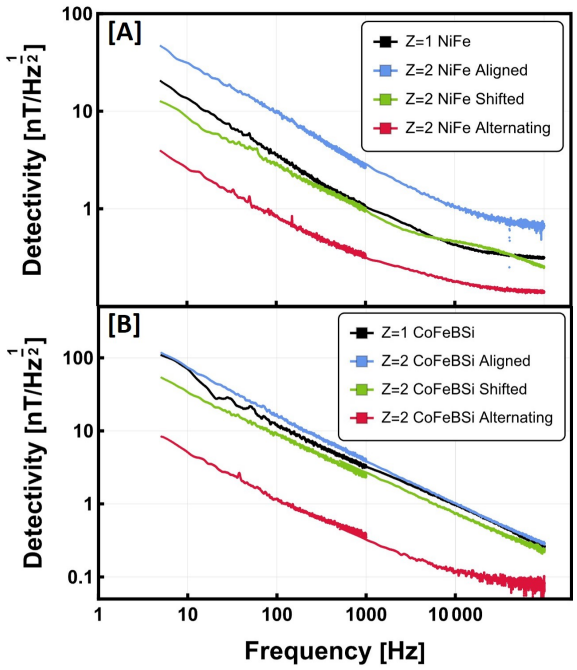


Fig. 5: Detectivity noise spectra of sensors with 200 MTJ arrays. [A] stack A sensors with a single TMR level ($n_Z$=1) and two levels connected in parallel ($n_Z$=2) for the various integration strategies. In [B] stack B sensors similarly.

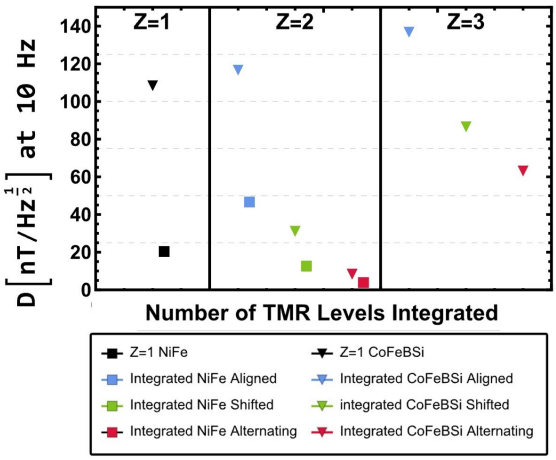


Fig. 6: Different detectivities at 10 Hz for 200 MTJs ($n_X$=20 and $n_Y$=10) sensor arrays with $n_Z$=1 and 2 for stack A and $n_Z$=1, 2 and 3 for stack B and the respective strategies.

result in lower detectivity in all frequency ranges compared with a single-level TMR sensor (excluding the RTN contribution in the shifted strategy). The aligned strategy shows higher detectivity due to the sensitivity loss (Fig. 3). The alternating strategy has the best detectivity performance, achieving lower noise levels while minimizing the MR loss inherent to the vertical integration process. However, this strategy also has the highest footprint among stacking strategies, with an area of 0.374 mm², compared to 0.300 mm² for the shifted strategy and 0.245 mm² for the aligned (or single-level) footprint.

| | Detectivity [nT·Hz$^{1/2}$] | | Footprint [mm$^2$] |
|---|---|---|---|
| | Stack A | Stack B | |
| **Z = 1** | 20.3 | 108.4 | 0.245 |
| **Z = 2 Aligned** | 46.6 | 116.6 | 0.245 |
| **Z = 2 Shifted** | 12.6 | 31.1 | 0.300 |
| **Z = 2 Alternating** | 3.9 | 8.3 | 0.374 |

Table I: Detectivity at 10 Hz and footprint of 200 MTJs array sensors for stack A and B, for the different integration strategies.

To further corroborate the potential for improving detectivity through vertical integration, Fig. 6 shows a lower detectivity for the shifted and alternating strategies, the latter achieving the lowest detectivity. Specifically, at 10 Hz with $n_Z$=2, stack A achieves a detectivity of 3.9 nT/Hz$^{1/2}$, and stack B of D = 8.3 nT/Hz$^{1/2}$. Moreover, additional integration of TMR levels may not necessarily impact on lowering the detectivity due to the sensitivity loss. This is evident by its increase in $n_Z$=3 of stack B when compared to $n_Z$=2, regardless of packing strategy.

Despite the decreased detectivity with some $n_z$=2 packing strategies, the final sensor footprint increases from aligned to shifted, and then alternating strategy. A summary of detectivity and the respective footprint of these strategies for 200 MTJs sensors is presented in table I. The sensor thickness will also increase proportional to $n_z$, which has low impact.

To validate the detectivity values estimated from the noise spectra, a varying magnetic field was applied with a set of Helmholtz coils. Fig. 7 shows the signal amplitude for different intensities of magnetic fields applied at 10 Hz for a sensor with $n_Z$=2 of the alternating strategy of stack A. From the decrease in amplitude with $H_{app}$ we have obtained a detectivity of at most 21.6 nT.Hz$^{-1/2}$, where the signal equals the background noise, showing coherence with the noise spectra measurement of 3.9 nT.Hz$^{-1/2}$.

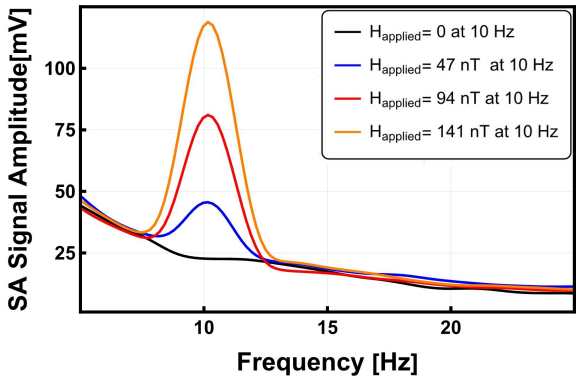


Fig. 7: Spectrum Analyzer (SA) signal amplitude for applied magnetic fields at 10 Hz of an alternating strategy sensor of stack A with $n_Z$=2. Resolution bandwidth was 2 Hz.

## IV. Conclusions

Through vertical integration of TMR levels, improved detectivity was achieved with appropriate strategies when compared to single-level TMR sensors ($n_Z$=1), specifically with the shifted and alternating approaches. The alternating strategy, in particular, significantly mitigates the sensitivity loss associated with vertical TMR integration, resulting in the lowest detectivity. For instance, in an array of 200 sensors with two vertical levels, stack A has detectivities of 3.9 nT.Hz$^{-1/2}$, while stack B reached 8.3 nT.Hz$^{-1/2}$. Despite its superior performance, the alternating strategy comes with a larger device footprint, 0.374 mm², compared to the shifted and aligned strategies, which have higher detectivities due to a poorer MR response.

Observing the detectivity evolution for sensors with stack B ($n_Z$=1, 2, and 3), the optimal packing occurs with two-level integration, specifically with the alternating strategy. This comes at the expense of a higher device footprint. The present strategy can be further extended when coupled with roughness mitigation strategies allowing more effective vertical packing.

## V. Acknowledgements

INESC MN acknowledges funding from FCT through BASE (UIDB/0536/2020) and PROGRAMATICO (UIDP/0536/2020) Programs. PDRA and FM acknowledge PD/BD/150391/2019 and UI/BD/151461/2021 grants, respectively. The work was partially supported by Agenda Microelectronica and GreenAuto Mobilising Agenda for Business Innovation, funded by the PRR and by European Funds NextGeneration EU and also MULTISPIN.AI project, through Horizon Europe Pathfinder program.

## References

[1] C. Zheng *et al.*, "Magnetoresistive sensor development roadmap (non-recording applications)," *IEEE Transactions on Magnetics*, vol. PP, pp. 1–30, Mar. 2019.

[2] D. Brisinda *et al.*, "Clinical magnetocardiography: The unshielded bet—past, present, and future," *Frontiers in Cardiovascular Medicine*, vol. 10, 2023.

[3] S. Cardoso, D. C. Leitao, L. Gameiro, *et al.*, "Magnetic tunnel junction sensors with ptesla sensitivity," *Microsystem Technologies*, vol. 20, no. 4-5, pp. 793–802, 2014.

[4] S. P. V. *et al.*, "A novel AMR based angle sensor with reduced harmonic errors for automotive applications," *Sensors and Actuators A: Physical*, vol. 324, 2021.

[5] M. Silva *et al.*, "Two-dimensional arrays of vertically packed spin-valves with picotesla sensitivity at room temperature," *Scientific Reports*, vol. 11, p. 215, 2021.

[6] R. Guerrero *et al.*, "Low frequency noise in arrays of magnetic tunnel junctions connected in series and parallel," *J. Appl. Phys.*, vol. 105(11), p. 113 922, 2009.

[7] A. Silva *et al.*, "Linearization strategies for high sensitivity magnetoresistive sensors," *The European Physical Journal Applied Physics*, vol. 72, Sep. 2015.

[8] M. D. Silva, "Novel architectures to integrate ultra sensitive sensors to detect biomedical signals," eng, Ph.D. dissertation, Jan. 2022, p. 143.

[9] E. Monteblanco *et al.*, "Normalization and correction factors for magnetic tunnel junction sensor performances comparison," *IEEE Sensors Journal*, vol. 21, no. 14, pp. 15 993–15 998, 2021.